International Journal of Scientific Research in Engineering and Management (IJSREM)
Volume: 10 Issue: 10 | Oct - 2026 SJIF Rating: 8.659 ISSN: 2582-3930

Enhanced UPQC Control for Power Quality Improvement in a Wave Energy-Driven PMSG System

L.Bhavani [1] T.Bhargavi [2], T. Rajeswari

[1]Electrical and Electronics Engineering & Holy Mary Institute of Technology and Science
[2]Electrical and Electronics Engineering & Holy Mary Institute of Technology and Science
[3]Electrical and Electronics Engineering & Holy Mary Institute of Technology and Science

---

Abstract—This paper presents a source-based study of unified power quality conditioner (UPQC) control for an oscillating-water-column wave-energy converter coupled to a permanent-magnet synchronous generator (PMSG). The architecture uses series and shunt voltage-source converters sharing a DC link. Frequency-fixed second-order generalized integrator (FFSOGI) quasi-type-1 phase-locked loops (QT1-PLLs) support phase estimation and sequence extraction; nonlinear proportional–integral (N-PI) control with feedforward supports DC-link regulation. The supplied documentation reports PSCAD/EMTDC comparisons for unbalanced nonlinear loads and voltage faults, including approximately 14 ms DC-link startup with the proposed control versus more than 40 ms for a conventional controller, and approximately 1.8% source-current THD under a reported disturbance case. Figures reproduced here originate from the supplied project document; no independent simulation or experimental verification has been performed.

Index Terms—Unified power quality conditioner, wave energy, PMSG, FFSOGI, phase-locked loop, nonlinear PI, harmonic compensation.

I. INTRODUCTION

Isolated coastal distribution systems can experience fluctuating generator voltage, unbalanced loading, nonlinear current distortion and reactive-power demand. The Bhavani documentation investigates a wave-energy-driven PMSG and locates a UPQC between the generator and sensitive loads. A series converter compensates voltage disturbances while a parallel converter mitigates harmonic and reactive currents. Their common DC-link requires tight regulation during disturbances.

The principal control elements reported in the source are a single-phase FFSOGI-QT1-PLL for per-phase sag/swell detection, a three-phase counterpart for positive-sequence extraction, and an N-PI DC-link regulator with a voltage-ratio feedforward term. The contribution of this manuscript is to organize the provided design and reported simulation evidence in IEEE paper form, not to claim a newly executed validation. An oscillating-water-column (OWC) wave-energy converter drives an air turbine and PMSG. The source describes measured torque and power inputs from Australian Maritime College model-pool tests, with a wave fluctuation period near 0.8 s

II. SYSTEM CONFIGURATION

The PMSG supplies three-phase nonlinear and inductive loads through the UPQC. A series voltage-source converter injects compensating voltage via coupling transformers; a shunt converter supplies compensating currents at the common coupling point.

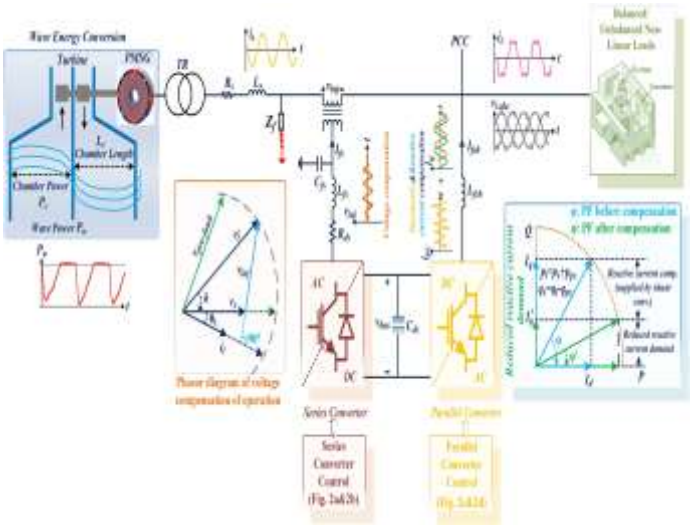


Fig. 1. Source-document OWC–PMSG and UPQC system architecture (reproduced from Bhavani documentation).

The empirical turbine relationship stated in the source is $T_m = \rho1(\Delta P)^2 - \rho2\Delta P$, with positive empirical coefficients ρ1 and ρ2. It links pressure drop to mechanical torque; numerical coefficient values are not supplied in the extracted documentation.

III. PROPOSED CONTROL METHODOLOGY

A. FFSOGI and phase synchronization: The in-phase and quadrature filters use a fixed nominal angular frequency ω0 and gain λs. Their transfer functions are $G\alpha(s) = \lambda s\omega0s/[s^2 + \lambda s\omega0s + \omega0^2]$ and $G\beta(s) = \lambda s\omega0^2/[s^2 + \lambda s\omega0s + \omega0^2]$. Fixed-frequency filtering allows the prefilter and PLL loop to be tuned separately. The source uses $\lambda s = \sqrt{2}$, a low-pass time constant of 5 ms, and PLL loop gain approximately 50, targeting a phase margin around 45°.

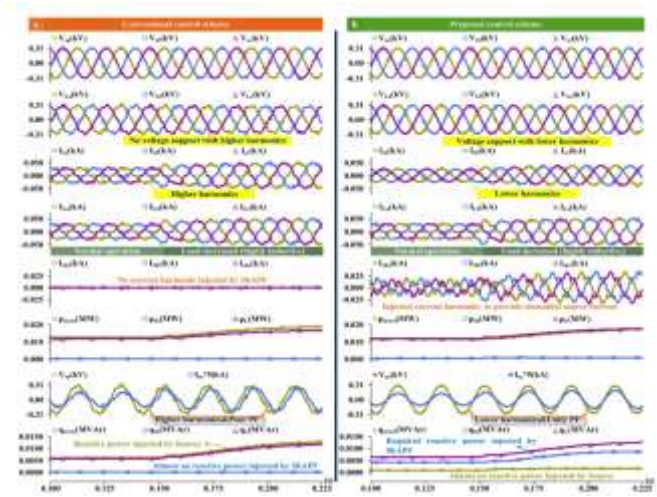


Fig. 2. Reported comparison waveforms for uncompensated and compensated operation (source figure).

B. Series converter: Per-phase voltage amplitude estimates identify sag or swell; reference injection voltage is formed from the difference between the desired positive-sequence load-voltage amplitude and the measured source amplitude. A PWM/hysteresis stage drives the series converter so the load-side voltage remains close to its reference during source-voltage disturbances.

C. Shunt converter: A three-phase FFSOGI-QT1-PLL extracts positive-sequence components. Harmonic, negative-sequence and reactive current components contribute to the reference compensating current. Current tracking is performed by the parallel converter, reducing distorted source currents and the reactive-power demand placed on the PMSG.

D. Nonlinear DC-link regulation: For voltage error e = Vdc − Vdc*, the document describes a nonlinear PI controller that increases corrective effort for large errors and suppresses ripple amplification near the reference. A feedforward current proportional to Δp = 1 − vsd/vld is added to account for voltage mismatch and converter power balance. This is a control-law description; exact reproduction requires the original gain set and executable model.

IV. SIMULATION MODEL AND TEST CONDITIONS

The source reports PSCAD/EMTDC evaluation using experimentally obtained WEC torque/power profiles. Test scenarios include nonlinear and highly inductive loads, load imbalance, abrupt load connection and single-/double-line-to-ground source faults. A later section of the same documentation separately describes a MATLAB/Simulink schematic labelled “wind generation.” Because that schematic does not unambiguously represent the wave-driven PMSG case, it is presented only as an additional illustrative UPQC implementation, not as verification of the PSCAD wave-energy results.

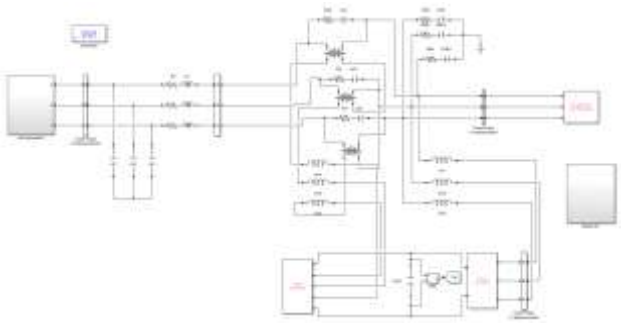


Fig. 3. MATLAB/Simulink UPQC schematic included in the documentation; wind-source label differs from the main wave-energy case.

V. RESULTS AND DISCUSSION

A. Dynamic voltage and current compensation: The documented results indicate that the series converter mitigates a reported 35% source-voltage sag during a double-line-to-ground fault while the shunt converter improves current symmetry and harmonic suppression. The waveforms show transitions between operating conditions; the figures should be read as previously reported source plots, not freshly generated simulation runs.

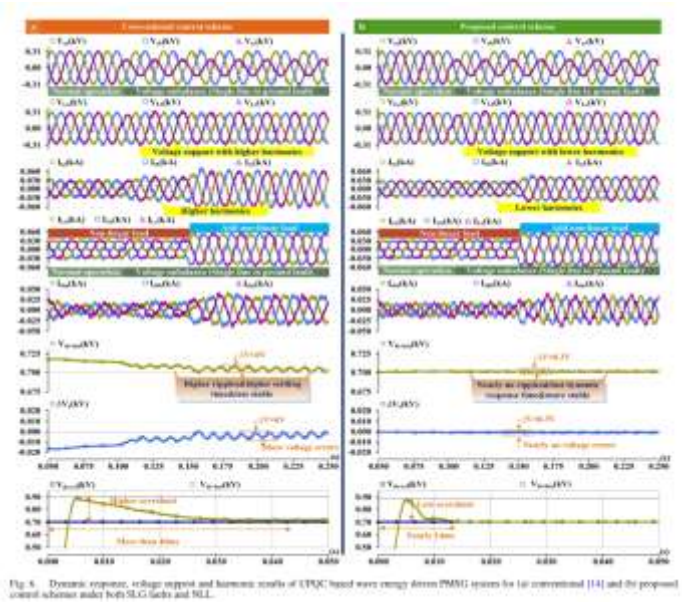


Fig. 4. Source-document dynamic waveforms for conventional and proposed control during disturbances.

B. DC-link regulation: The documentation reports an approximate 14 ms startup response with the proposed N-PI control versus over 40 ms under conventional control. It further states a startup tracking error around 0.3 V and a disturbance steady-state deviation around 0.2 V. The stated figures are retained as reported; raw time-series data and complete model parameters were not provided for independent re-computation.

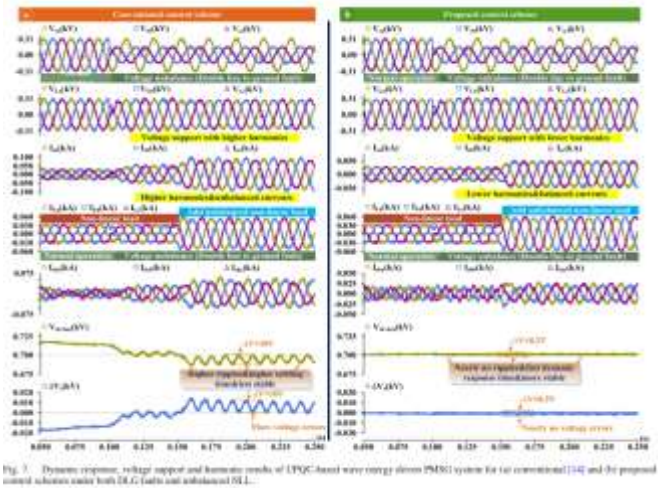


Fig. 5. Source-document comparative simulation waveform set.

C. Harmonic performance: Under a reported unbalanced-load and fault test, source-current THD is stated to be approximately 1.8% and power factor nearly unity. Another source comparison describes source-current THD in the approximate range 1.5–2.0%. A rigorous IEEE 519 compliance determination also depends on measurement location, current-demand ratio and applicable limits; therefore the numerical THD values alone should not be treated as a complete standards audit.

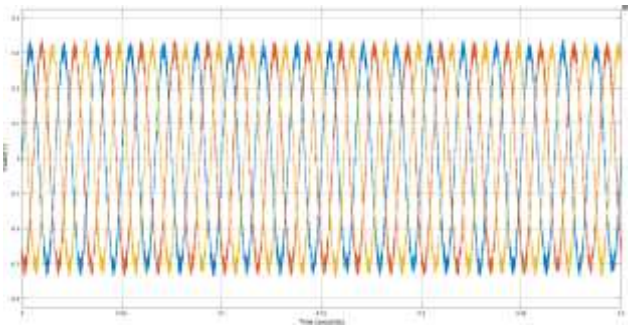


Fig. 6. Additional simulation scope waveform reproduced from the project documentation.

V-A. WAVE-ENERGY INPUT AND ELECTROMECHANICAL COUPLING

The source documentation uses a unidirectional air turbine driven by an oscillating-water-column chamber. Alternating wave-induced chamber pressure is converted to mechanical torque, and the PMSG converts this torque to electrical power. The stated experimental wave fluctuation period is approximately 0.8 s. Such periodic input is important because the source voltage and generator power may vary even when the connected electrical load is unchanged. In the simulation narrative, measured torque and power traces from a model test pool provide the mechanical excitation. However, the underlying numeric sample records and turbine identification coefficients are not included in the supplied paper material.

For a generic rotor model, $J(d\omega m/dt) = Tm - Te - B\omega m$, where J is combined rotational inertia, ωm mechanical angular speed, Te electromagnetic torque and B the viscous damping coefficient. This is a standard modeling relation included here to clarify the mechanical-to-electrical pathway; it is not presented as a separately validated equation fitted to the supplied experimental traces. In a PMSG, the electrical frequency and induced voltage depend on machine operating conditions, so disturbances propagate to the voltage-conditioning stage unless actively compensated.

V-B. SYNCHRONIZATION AND SEQUENCE SEPARATION

The frequency-fixed second-order generalized integrator produces orthogonal in-phase and quadrature outputs, supporting fundamental-frequency estimation even when measured voltages contain harmonics. Unlike frequency-adaptive structures, the nominal angular frequency remains fixed in the prefilter, permitting independent selection of the SOGI and PLL tuning gains. The quasi-type-1 PLL uses the filtered components to estimate phase and voltage amplitude. The supplied documentation selects a nominal half-cycle averaging equivalent to 10 ms at 50 Hz and a 5 ms low-pass time constant. The loop gain is reported as 50 with an approximately 45-degree phase margin. These are source-reported design choices rather than newly optimized settings.

The single-phase path is applied separately to phases a, b and c. This is useful for detecting phase-selective voltage faults: the estimated per-phase positive-sequence magnitude is compared with the desired reference, and the difference determines the injection command. In the three-phase path, Clarke-transformed αβ voltages and currents are separated into positive and negative sequence components. The positive-sequence fundamental current supports a balanced source-current reference; negative-sequence, harmonic and reactive components are assigned to the shunt converter for compensation.

$$v_{ser,x}(t) = \sum_{k=s^+} V_k \cos(\omega t + \varphi_k), \qquad (2)$$

Fig. 7. Source-provided UPQC controller architecture with PLL, series and shunt control blocks.

V-C. SERIES-CONVERTER VOLTAGE SUPPORT

A series converter must restore the load voltage when the generator-side voltage is depressed or elevated. The documentation computes a voltage-injection reference using the desired positive-sequence load-voltage magnitude and the measured phase voltage. A voltage deviation threshold of approximately ±10% is discussed in the source as a control trigger. During a sag, the injected voltage adds to the source voltage; during a swell, the converter produces a compensating opposing voltage. The available injection magnitude depends on converter and DC-link ratings, which must be specified for any final implementation.

For phase x, a useful idealized statement is $v_{L,x}(t) = v_{s,x}(t) + v_{inj,x}(t)$. Accordingly, the reference $v_{inj,x}^*(t) = v_{L,x}^*(t) - v_{s,x}(t)$ indicates the commanded series voltage. This identity

explains the compensation objective but does not reproduce all switching and transformer dynamics. The controller output is converted to gate pulses by the PWM/hysteresis implementation shown in the source. A complete replication would additionally require the transformer turns ratio, filter inductance, switching frequency, sampling time and saturation constraints.

V-D. SHUNT-CONVERTER CURRENT COMPENSATION

The parallel converter aims to prevent nonlinear load-current distortion and reactive demand from appearing at the PMSG terminals. It synthesizes a compensating current equal to the difference between the load current and the desired source current, subject to the selected sign convention. The desired source current follows the fundamental positive-sequence voltage and is therefore balanced and close to in phase with the source. The reference also incorporates a DC-link power-balancing component, so current compensation and capacitor-voltage regulation are coupled.

Instantaneous active and reactive power can be evaluated in the αβ stationary frame as p = vαiα + vβiβ and q = vαiβ − vβiα. The documentation uses reactive-current control to offset load reactive power and also describes an active-current feedforward contribution based on the voltage ratio between source and load. These elements explain why the UPQC is able to address both power factor and harmonics, unlike a series-only voltage compensator.

$$G_{ip} = \frac{V_{ser,x,ip}}{V_{ser,x}} = \frac{\lambda_s \bar{\omega} s}{s^2 + \lambda_s \bar{\omega} s + \bar{\omega}^2}. \quad (3)$$

$$G_{qp} = \frac{V_{ser,x,qp}}{V_{ser,x}} = \frac{\lambda_s \bar{\omega}^2}{s^2 + \lambda_s \bar{\omega} s + \bar{\omega}^2}. \quad (4)$$

Fig. 8. Additional source figure illustrating PLL tuning and transient phase estimation.

V-E. NONLINEAR PI AND FEEDFORWARD POWER BALANCE

A conventional PI controller applies proportional and integral actions directly to the DC-link tracking error. Under a sudden voltage sag or load change, a large proportional gain may accelerate recovery but amplify ripple and overshoot near steady state. The nonlinear PI formulation in the documentation instead applies an error-dependent nonlinear mapping, parameterized by μ and ε, to the proportional and integral terms. Small errors produce reduced control effort, while larger errors elicit stronger correction. The source describes μ = 1 as the linear PI limiting case. The DC-link energy relation is E = (1/2) CdcVdc² and dE/dt = Pinput − Poutput − Ploss. Consequently, transient changes in converter power exchange perturb Vdc. A feedforward current term based on Δp = 1 − vsd/vld is included to anticipate the power imbalance caused by unequal source and load voltages. The exact closed-loop response is influenced by capacitance, converter losses, control delays and gain selection. Because the supplied file does not provide a complete machine-readable model, this paper preserves the reported controller principle without asserting a fresh numerical optimization.

V-F. SIMULATION SCENARIOS AND EVALUATION METRICS

The simulation narrative describes operation under unbalanced and highly inductive nonlinear loads, abrupt load connection, voltage sag and swell, and single-line-to-ground or double-line-to-ground faults. These cases stress different functions of the UPQC. Nonlinear loads test current-harmonic cancellation; inductive loading tests reactive compensation; unbalance tests sequence extraction; faults test voltage restoration; and abrupt transitions test DC-link stability. For meaningful comparison, both conventional and proposed controllers must use identical source, load, fault and switching conditions.

The principal reported performance metrics are source-current total harmonic distortion (THD), load-voltage regulation, phase synchronization response, source power factor, DC-link settling time and DC-link voltage deviation. THD should be calculated from an identified harmonic analysis window as THD = sqrt(sum from h=2 to H of Ih²)/I1 × 100%. The source reports approximate THD outcomes but does not provide every harmonic bin or the underlying waveform export. Therefore, these metrics are summarized as reported outcomes, not recomputed measurements.

$$G_{qsg}(s) = 1/(\tau_q s + 1), \quad (5)$$

Fig. 9. Source-provided nonlinear control function illustrating error-dependent controller response.

V-G. COMPARATIVE INTERPRETATION OF REPORTED WAVEFORMS

In the source plots, the uncompensated or conventional-control traces show larger current distortion and less desirable transient behavior, whereas the proposed controller traces indicate improved current balance and faster DC-link regulation. The reported DC-link startup response of about 14 ms versus greater than 40 ms for a conventional control scheme suggests faster transient recovery under the modeled conditions. The reported source-current THD of approximately 1.8% is also consistent with the stated harmonic mitigation objective. These values should not be generalized to different converter ratings, sea states or fault depths without additional testing. The waveform panels also illustrate a key tradeoff: voltage compensation is achieved by injecting power through the series branch, while the shunt branch and DC capacitor must sustain the resulting energy exchange. Thus, strong voltage restoration can impose transient current and DC-link demands. The feedforward and nonlinear regulator seek to reduce that interaction. For publication-quality reproducibility, future results should present a table of exact numerical values and matched waveforms for each test case, with converter ratings and measurement definitions.

V-H. REPRODUCIBILITY AND STANDARDS CONSIDERATIONS

The documentation refers to IEEE Std 519 in discussing current harmonic performance. A complete compliance assessment requires identifying the point of common coupling, voltage level, individual harmonic limits and the ratio of available short-circuit current to maximum demand load current. A low THD percentage is encouraging but does not by itself establish full compliance with every applicable current-distortion criterion. Similarly, power factor and voltage regulation should be stated with clear averaging intervals and nominal voltage bases.

A reproducible study should archive the PSCAD/EMTDC project, turbine input time series, PMSG electrical and mechanical ratings, series transformer data, shunt/series filters, DC-link capacitance, PWM switching settings, sampling time, fault impedances, nonlinear load configuration and complete controller gains. The supplied documentation also contains a separate wind-labelled MATLAB/Simulink schematic. That image is retained as a source illustration but should not be interpreted as an identical validation of the OWC wave-driven PMSG simulation.

V-I. IMPLEMENTATION SEQUENCE AND SIGNAL FLOW

The model implementation follows a causal signal flow. First, the mechanical input drives the PMSG, establishing the instantaneous generator terminal voltages and currents. Next, the controller measures the three source voltages, three load voltages, three load currents and common DC-link voltage. The single-phase synchronization branches process each source voltage independently; the three-phase branch processes the αβ voltage and current signals. This separation allows voltage fault detection to proceed independently of the harmonic-current reference generation. In the source description, filtering, reference formation and switching generation operate as coupled but identifiable subsystems.

At each control interval, the series controller compares the estimated source voltage magnitude with the desired load-voltage reference and creates an injection command when compensation is required. Simultaneously, the shunt controller forms a balanced positive-sequence source-current target, subtracts the measured load current to obtain the compensation requirement and adds a DC-link regulating current contribution. The switching controller translates these references into voltage-source-converter gate signals. The coupling transformer and passive filters then transfer the corrective voltage and current to the electrical network. These steps are an explanatory reconstruction of the control architecture in the documentation, not a claim that an executable simulation model was rebuilt. Controller initialization and protection are important in practical implementation. A voltage-source converter cannot be safely commanded without DC-link precharge, measurement validation and current limiting. During deep voltage faults, the required series injection may exceed the available converter voltage, while the shunt branch may be constrained by semiconductor current ratings. An implementation therefore needs saturation logic, anti-windup for integral states, overvoltage and undervoltage thresholds, and coordinated fault handling. The supplied documentation emphasizes transient performance but does not give a complete protection state machine; these implementation requirements are identified here as engineering considerations rather than documented experimental features.

For computational evaluation, an appropriate sampling interval must resolve both the fundamental waveform and the converter switching dynamics. A slow time step may underestimate current ripple, miss switching transients and distort harmonic measurements; an unnecessarily small step increases computational cost. Simulation solver settings should be reported together with switching frequency, current control hysteresis band, numerical integration method and transient initialization. The supplied material does not specify all such settings in a single reproducibility table. Accordingly, exact numerical replication remains outside the scope of this manuscript.

V-J. FAULT RESPONSE AND TRANSIENT ANALYSIS

The voltage sag test described in the source probes whether the per-phase PLL can detect a source disturbance quickly enough for the series converter to prevent substantial load-voltage depression. A single-line-to-ground fault produces asymmetric phase conditions and can generate negative-sequence voltage; a double-line-to-ground fault can introduce deeper phase-specific disturbances. In both cases, balanced three-phase assumptions are inadequate for fault detection, which motivates the use of separate single-phase estimators for the series converter. The source states that the proposed phase estimator responds faster to a −0.4 p.u. sag than selected comparator PLL techniques.

The source also discusses a 35% source-voltage sag under a double-line-to-ground condition. The reported compensating waveforms illustrate the expected physical action: the series converter injects the missing voltage while the load-side voltage remains closer to its desired amplitude. This behavior is constrained by converter power balance and by the magnitude of the fault. The source figure alone does not establish a universal restoration guarantee for arbitrary fault impedances or durations. Quantitative evaluation would require time-aligned traces of source voltage, injection voltage, load voltage, DC-link voltage and shunt current for the same fault interval.

A sudden load connection is a complementary test because it changes active and reactive demand without necessarily changing the upstream source voltage in the same way as a fault. Under inductive loading, the shunt converter must provide reactive current to avoid excessive generator reactive demand. Under nonlinear loading, it must also provide harmonic currents. These simultaneous objectives compete for

converter current capacity. The proposed positive-sequence extraction and nonlinear DC-link control are intended to improve coordination, but the documentation does not report a complete converter-current margin for each operating case.

$$\angle G_{ip}(j\omega) \approx -\frac{\omega^2-\bar{\omega}^2}{\lambda_s\omega\bar{\omega}} \approx -\frac{2}{\lambda_s\bar{\omega}}\tilde{\omega} \approx \tau_0\tilde{\omega},$$
$$|G_{ip}(j\omega)| \approx (\lambda_s\omega\bar{\omega})/\sqrt{(\bar{\omega}^2-\omega^2)^2+(\lambda_s\omega\bar{\omega})^2}. \quad (6)$$

Fig. 10. Source-document plot associated with controller and operating-condition analysis.

V-K. POWER QUALITY INTERPRETATION

Power quality is a multi-dimensional requirement. Voltage amplitude regulation, current waveform distortion, phase balance, reactive power exchange and transient recovery are related but distinct. A UPQC addresses these by dividing the responsibilities between series and shunt converters. The series path primarily regulates the voltage experienced by the load, while the shunt path shapes the current seen by the generator. The common DC link provides the power-exchange mechanism connecting the two. As a result, performance cannot be assessed from a single THD value or one voltage trace alone.

The reported near-unity source power factor suggests that the shunt controller successfully offsets much of the reactive current required by the inductive load under the documented case. Nevertheless, the numerical power-factor value, the precise load impedance and the averaging method must be available to reproduce that conclusion. Likewise, source-current THD is meaningful only when the fundamental current magnitude and harmonic measurement window are specified. A particularly low fundamental current can make THD sensitive to small absolute harmonic currents. These qualifications matter when comparing control methods across different loading conditions.

The wave-energy source also introduces an important separation between slow mechanical variability and fast electrical compensation. The approximately 0.8 s wave fluctuation described in the documentation is much slower than the nominal 20 ms period of a 50 Hz electrical waveform, but it can still affect voltage amplitude and available active power. The controller therefore operates across different time scales: the PLL estimates fundamental phase, current control reacts to harmonic and load disturbances, and DC-link regulation balances converter energy. This multiscale perspective helps interpret why a fast DC-link transient response is useful even when the wave input itself changes more slowly.

V-L. RECOMMENDED EXPERIMENTAL VALIDATION

Before journal submission, the reported waveforms should be validated with a repeatable protocol. A baseline run without UPQC should be compared against a conventional UPQC controller and the proposed FFSOGI-QT1-PLL/N-PI controller under identical wave input and load conditions. Each run should use the same initial DC-link voltage, converter ratings, disturbance start and end times, and harmonic analysis windows. The report should tabulate load-voltage RMS deviation, source-current THD, reactive power, power factor, DC-link peak overshoot, settling time and maximum compensating current. These additional measurements are proposed validation steps and are not fabricated findings.

A parameter-sensitivity experiment should vary SOGI gain, PLL loop gain, nonlinear PI parameters and DC-link capacitance. This would test whether the reported improvements remain robust when model settings depart from their nominal values. A separate frequency-deviation test would be particularly relevant because a frequency-fixed SOGI may introduce phase and amplitude estimation errors when generator frequency changes. Finally, a hardware-in-the-loop setup could test real-time computation, measurement noise, converter saturation and controller delays. Such experiments would strengthen the evidence beyond the source-reported PSCAD plots.

VI. LIMITATIONS AND FUTURE WORK

The provided document does not establish a single reproducible dataset across its PSCAD wave-energy study and the separate wind-labelled Simulink model. Raw simulation project files, detailed converter ratings, full controller gains, harmonic FFT tables and time-stamped numeric waveform exports would be required for independent validation. Future work can include wave/wind model separation, parameter sensitivity studies, energy-storage-assisted DC-link control, frequency-adaptive synchronization, real-time hardware-in-the-loop testing and systematic fault ride-through benchmarking.

VII. CONCLUSION

The supplied project evidence supports the usefulness of coordinated series and shunt UPQC control in a wave-energy-driven PMSG architecture. FFSOGI-QT1-PLL synchronization, positive-sequence extraction and nonlinear DC-link regulation are the central reported design features. Documented simulations show improved voltage disturbance mitigation, source-current quality and DC-link transient response compared with conventional control. These are source-reported outcomes and require model-level replication before being represented as new independent experimental findings.

REFERENCES

[1] Bhavani, “Improved UPQC Control System for Wave Energy-Powered PMSG System Power Quality Enhancement,” project documentation supplied by the author, undated.

[2] H. Akagi, E. H. Watanabe, and M. Aredes, Instantaneous Power Theory and Applications to Power Conditioning, 2nd ed. Hoboken, NJ, USA: Wiley-IEEE Press, 2017.

[3] A. Ghosh and G. Ledwich, Power Quality Enhancement Using Custom Power Devices. Boston, MA, USA: Kluwer Academic, 2002.

[4] V. Khadkikar, "Enhancing electric power quality using UPQC: A comprehensive overview," IEEE Trans. Power Electron., vol. 27, no. 5, pp. 2284–2297, May 2012.

[5] H. Fujita and H. Akagi, "The unified power quality conditioner: The integration of series- and shunt-active filters," IEEE Trans. Power Electron., vol. 13, no. 2, pp. 315–322, Mar. 1998.

[6] P. Rodríguez et al., "Grid synchronization of power converters using multiple second order generalized integrators," in Proc. 34th Annu. Conf. IEEE Ind. Electron. Soc. (IECON), 2008, pp. 755–760.

[7] F. Blaabjerg, R. Teodorescu, M. Liserre, and A. V. Timbus, "Overview of control and grid synchronization for distributed power generation systems," IEEE Trans. Ind. Electron., vol. 53, no. 5, pp. 1398–1409, Oct. 2006.

[8] IEEE Std 519-2022, IEEE Standard for Harmonic Control in Electric Power Systems. IEEE, 2022.

[9] J. Falnes, Ocean Waves and Oscillating Systems: Linear Interactions Including Wave-Energy Extraction. Cambridge, U.K.: Cambridge Univ. Press, 2002.

[10] A. F. de O. Falcão, "Wave energy utilization: A review of the technologies," Renew. Sustain. Energy Rev., vol. 14, no. 3, pp. 899–918, 2010.